# Comparison of laser induced breakdown spectroscopy and fast ICCD imaging for spatial and time resolved measurements of atmospheric pressure helium plasma jet

# QUERY FORM

JOURNAL: Plasma Sources Science and Technology

AUTHOR: D Maletić *et al*

TITLE: Comparison of laser induced breakdown spectroscopy and fast ICCD imaging for spatial and time resolved measurements of atmospheric pressure helium plasma jet

ARTICLE ID: ac4ddd

---

Your article has been processed in line with the journal style. Your changes will be reviewed by the Production Editor, and any amendments that do not comply with journal style or grammatical correctness will not be applied and will not appear in the published article.

The layout of this article has not yet been finalized. Therefore this proof may contain columns that are not fully balanced/matched or overlapping text in inline equations; these issues will be resolved once the final corrections have been incorporated.

---

Q1: Please check that the names of all authors as displayed in the proof are correct, and that all authors are linked to the correct affiliations. Please also confirm that the correct corresponding author has been indicated. Note that this is your last opportunity to review and amend this information before your article is published.

Q2: If an explicit acknowledgment of funding is required, please ensure that it is indicated in your article. If you already have an Acknowledgments section, please check that the information there is complete and correct.

Q3: Please check that the funding information below is correct for inclusion in the article metadata.
Ulster University, U.K.
Ministry of Education, Science and Technological Development, Republic of Serbia 451-03-68/2020-14/200024
Centre of Excellence Non Equilibrium Processes, IPB
European Cooperation in Science and Technology TD1208
Croatian Science Foundation HrZZ, Croatia IP-2013-11-2753 IP-2019-04-6418
Serbian Academy of Sciences and Arts F155

Q4: We have been provided with ORCID iDs for the authors as below. Please confirm whether the numbers are correct.
Dejan Maletić 0000-0002-0368-6568
Dean Popović0000-0003-3906-3482
Zoran Lj Petrović 0000-0001-6569-9447
Slobodan Milošević 0000-0002-4455-7869

Q5: Please be aware that the colour figures in this article will only appear in colour in the online version. If you require colour in the printed journal and have not previously arranged it, please contact the Production Editor now.

Q6: Please specify the corresponding author and provide their email address.

Q7: Please define the acronym for 'ICCD'.

Q8: Please define the acronym for 'CCD'.

Q9: Please define the acronym for 'HV'.

Q10: A standard data availability statement has been added to your article, based on the information you gave in your submission. This text cannot be changed unless there is an error. Please remove any other data statement if the information is now duplicated. If the standard statement includes a link or DOI, please check that this is also an item in the reference list. If not, please provide the reference details (author, year, data title, repository name, link) and indicate where this reference should be cited in the text of your article.

Q11: Reference [2] in your original source file was a duplicate of [1] and hence the repeated version has been deleted from the proof. Please check.

Q12: Please provide the initials for the authors [Oh, Szili, Hatta, Ito and Shirafuji] in reference [12].

IOP Publishing Plasma Sources Science and Technology
Plasma Sources Sci. Technol. **0** (2022) 000000 (10pp) https://doi.org/10.1088/1361-6595/ac4ddd

# Comparison of laser induced breakdown spectroscopy and fast ICCD imaging for spatial and time resolved measurements of atmospheric pressure helium plasma jet

**Dejan Maletić[1,2], Dean Popović[2], Nevena Puač[1], Zoran Lj Petrović[3,4] and Slobodan Milošević[2]**

[1] Institute of Physics, University of Belgrade, Pregrevica 118, 11000 Belgrade, Serbia
[2] Institute of Physics, Bijenička 46, 10000 Zagreb, Croatia
[3] Serbian Academy of Sciences and Arts, Knez Mihajlova 35, 11001 Belgrade, Serbia
[4] School of Engineering, Ulster University, Jordanstown, Co. Antrim, BT37 0QB, United Kingdom

E-mail: dejan_maletic@ipb.ac.rs, dmaletic@ifs.hr and z.petrovic@ulster.ac.uk

Received 21 October 2021, revised 13 December 2021
Accepted for publication 21 January 2022
Published XX XX XXXX

**Abstract**

In this paper we compared the fast ICCD imaging with the newly developed diagnostic method that utilizes laser induced breakdown in plasma jet. Our helium plasma jet was powered by an 80 kHz high-voltage sine wave and propagated into the ambient air. Pulsed laser beam 1064 nm (4 ns pulse duration and 5 Hz repetition rate) was focused with the lens into the plasma jet at energy below breakdown threshold in helium. Laser pulses and the jet powering signal were synchronized. Laser induced plasma is highly dependent on the concentration of seed electrons and other charged particles in the plasma jet channel. We compared the radial profiles of the plasma jet obtained with these two methods. For laser induced breakdown it was $\pm 0.5$ mm and for ICCD measurement it was $\pm 1.75$ mm, while the ionization wave velocities obtained with these two methods were 15 km $s^{-1}$ and 20 km $s^{-1}$ respectively. Electrical characteristics of the plasma jet were also presented and one can see a large hysteresis effect when the applied power to the plasma jet was reducing. We show that the laser induced breakdown spectroscopy can be used as a complementary diagnostics technique with ICCD measurements.

Keywords: DBD plasma jet, laser induced plasma, LIP, ICCD imaging, helium plasma jet

(Some figures may appear in colour only in the online journal)

## 1. Introduction

Atmospheric pressure plasma jets (APPJs) attract a lot of attention due to their great range of possible applications especially in biotechnologies and medicine [1]. The primary requirement for treatments of living cells and tissues is the non-equilibrium nature of those plasmas. Due to a variety of specific applications, it is necessary to study in detail all physical and chemical processes, both in the plasma jet itself and in its interaction with the treated samples. To solve these complex problems many diagnostics techniques are used such as optical emission spectroscopy (OES), mass spectrometry, Schlieren imaging, laser induced fluorescence (LIF), electrical probe measurements, cavity ring down spectroscopy [2–6]. From the fast ICCD imaging it was found that plasma jets are not continuous but consist of fast-moving self-propagating ionization waves (IWs). The head of the plasma jet is loaded with a high concentrations of highly reactive species. The most important reactive

* Author to whom any correspondence should be addressed.

 

species in plasma jets are reactive oxygen nitrogen species (RONS), ions, electrons and UV radiation. Commonly used gases as flowing buffers for plasma jets are helium and argon [7–10]. The main RONS are hydroxyl radical •OH, ozone $O_3$, $NO_x$, $N_2^+$, $O^-$ and others [8, 11, 12]. A large percentage of research in plasma medicine is done by using plasma jets, because of their simple construction and flexible range of operating parameters. Plasma jets are used for bacteria sterilization, carcinoma cell treatment, blood coagulation and other [13–15]. Treatment by a single plasma jet is usually limited to 1 $cm^2$, so for larger surfaces, plasma jets can be connected in arrays of several identical plasma jets [16–18]. One of the new emerging fields in plasma jet applications is treatment of water and production of plasma activated water [12, 19–22] or medium [23, 24].

Medical and biotechnology applications of plasmas [25, 26] have opened a large activity in the field and it became necessary to understand those plasmas better in order to interpret and optimize those applications. Having in mind all the difficulties encountered in diagnostics of atmospheric pressure plasmas each new result is valuable especially when more than one technique has been applied and results are tested for consistency.

In this work we compared two very different plasma diagnostic techniques. The first is broadband fast ICCD imaging that is a non-perturbing technique and the second laser induced breakdown spectroscopy (LIBS) that is the opposite, a perturbing technique. Laser induced breakdown in gases has been studied in the first decades of laser applications, followed by the development of LIBS, a versatile technique for elemental analysis of solid materials [27, 28], as well as liquid [29] and gas/aerosols [30]. For the breakdown to occur in a gas, a critical electron density needs to be reached in the laser focal volume. For relatively lower laser intensities, this can occur via two processes, multiphoton ionization and laser induced avalanche ionization. In general, the individual contribution of those two processes depends on the laser wavelength and pulse duration. Using shorter wavelengths and shorter pulses leads to higher probability of multiphoton ionization to occur (especially with femtosecond lasers). In contrast to that, laser induced avalanche ionization favours longer pulses further in the infrared. Most importantly, this is a process that involves free electrons and is thus an ideal candidate for their detection. Theoretically, the process begins with a certain low electron density (at least a single electron) in the laser focal volume, which is then increased by a repeated inverse bremsstrahlung and electron impact ionization [31]. The detection threshold (lowest electron density detectable) can easily be changed by changing the laser pulse energy, so the occurrence of a laser induced plasma (LIP) corresponds to a certain electron density at the beginning of the laser pulse. This concept was first shown in a publication by Popović *et al* where a nanosecond Nd:YAG laser was used to detect free electrons in a helium APPJ via laser induced avalanche ionization [32]. More recently, Woodbury *et al* showed that low concentrations of charged species can be probed by using a picosecond mid-infrared laser for avalanche ionization breakdown of air [33]. The charged species were a result of nearby radioactive source. The authors also discussed the implementation of this technique for low-density plasma detection.

Here we will show similarities and differences of these two techniques for the plasma jet diagnostics. For example, one of the first observables to be recorded in such plasmas were the velocities of propagation of ionization fronts. Those are considerably different from the plasma flow velocities and are a projection of the space charge formation and propagation. Most of the results were obtained by using ICCD and there is wealth of data on how these velocities vary with different parameters [34–37]. Here we compared the ICCD data to those obtained by the laser induced breakdown measurements for sinewave excitation signal.

## 2. Experimental setup

In this paper we used two experimental setups, the first setup was for the LIBS experiment (see figure 1(a)) and the second setup for the ICCD measurements (see figure 1(b)). There are some differences in the used experimental equipment between these two experiments because they are performed in collaboration of two laboratories. The differences are such that they cannot affect the nature of the final results. The plasma jet electrode configuration and power supply for the plasma jet are the same. ICCD measurements were carried out at the Institute of Physics in Belgrade (Serbia) and the experiment on the LIBS in plasma jet was performed at the Institute of Physics in Zagreb (Croatia). Plasma jet is made of a capillary glass tube with the inner diameter (I.D.) of 1 mm and the outer diameter of 6 mm. The two external electrodes were made of copper foil wrapped around the glass tube. The width of the electrodes, the electrode gap and the distance of the first electrode from the edge of the glass tube were all 10 mm. The electrode closer to the plasma jet nozzle was connected to the high voltage power supply. The second electrode was connected to the ground through a resistor of 100 kΩ. The high voltage power supply was modular and consisted of the signal generator (PeakTech DDS Function Generator 4025 used for ICCD measurements and Keysight Arbitrary Waveform Generator 33522B used in laser measurements), custom made amplifier and a high voltage transformer. The operating frequency of the plasma jet was 80 kHz (unit time cycle 12.5 micro-seconds). High purity helium 5.0 (99.999%, Messer) was used as the working gas. The flow rate of 2 l $min^{-1}$ of the working gas was set by a mass flow controller (Bronkhorst MASS-VIEW® MV-196-HE or Alicat MC-5SLPM-D). The electrical properties of the discharge were measured by high voltage (Tektronix P6015A, 75 MHz bandwidth) and current (Pearson 2877) probes. Waveforms were acquired by oscilloscope (Picoscope 5244B). LIP was produced by a Q-switched Nd-YAG laser at 1064 nm (Quantel Brilliant, pulse width 4 ns) operating typically at the repetition rate of 5 Hz. Polarizing beam splitter cube (CCM1-PBS25-1064-HP/M, Thorlabs) was used for attenuation of the laser power. Laser beam was focused on the helium plasma jet at 5 mm below the capillary nozzle using a fused silica lens with antireflection coating (focal length 5 cm, diameter 2.5 cm). For the laser energy measurement, we used laser

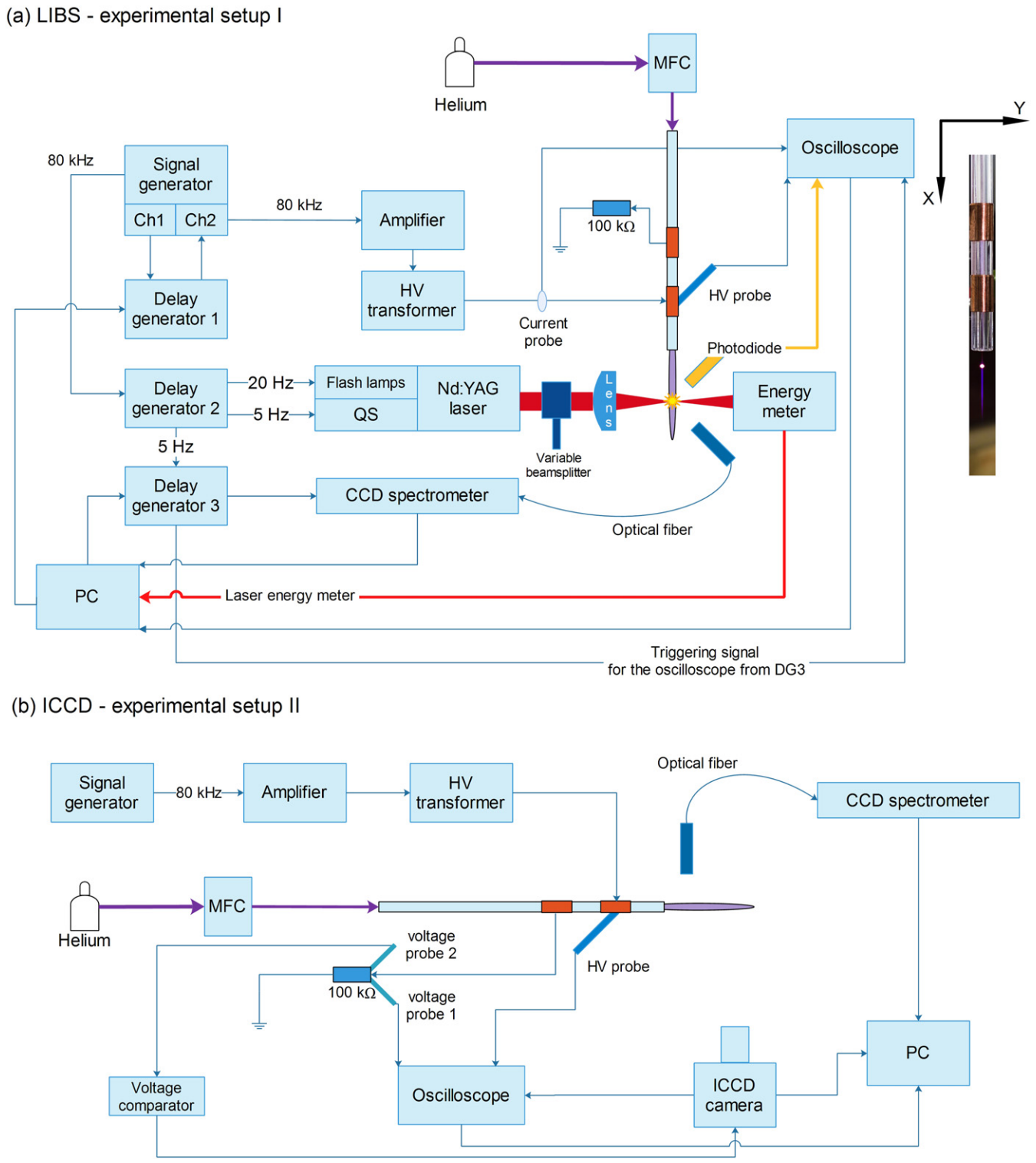


**Figure 1.** Experimental setups: (a) LIBS and (b) ICCD.

energy meter (PE25BB-DIF-SH, Nova II, Ophir) at 15 cm after the lens focus. Laser delivered energy to the plasma jet was 20 mJ which was below breakdown threshold in helium at atmospheric pressure under present excitation conditions. The threshold for the laser plasma breakdown was experimentally determined by slowly reducing the applied laser energy, and when the laser plasma disappear that was the energy that we used in LIBS experiment.

The laser synchronization with the high voltage signal and spectrometer was achieved by using three digital delay generators (Stanford Research Systems 645). A signal generator was used as the master device. Signal generator controlled delay

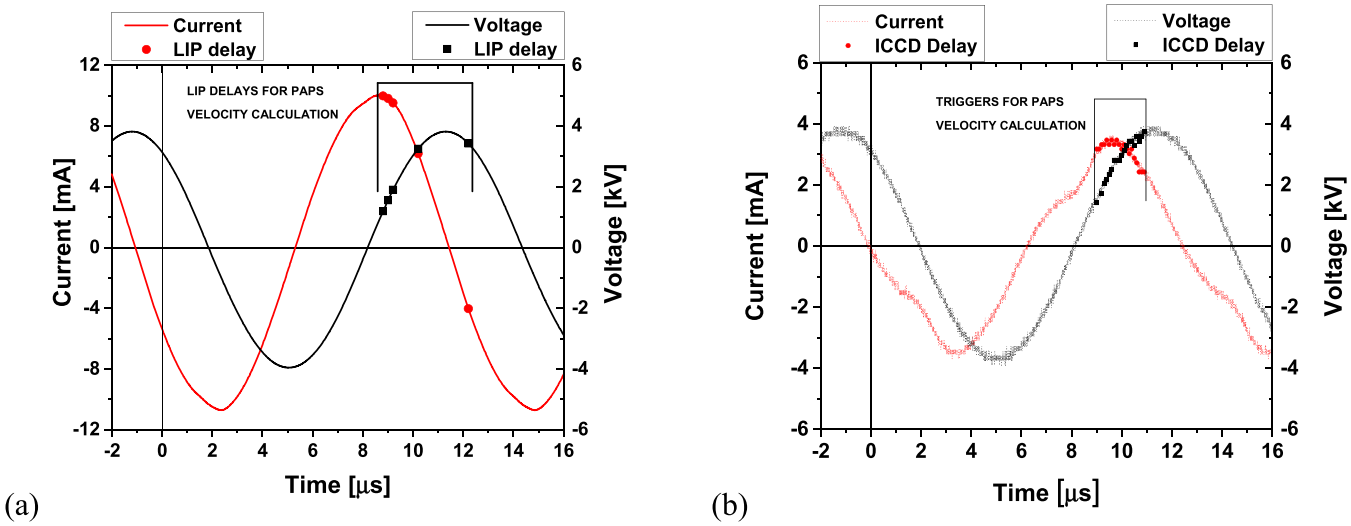


**Figure 2.** Typical waveforms of the plasma jet discharge (a) Current and voltage signals for the plasma jet measured at the high voltage powering cable. (b) Current and voltage signals for the plasma jet discharge, current was measured as the voltage drop at the 100 kΩ resistor. ICCD camera delay range with the step of 0.1 $\mu$s for calculating the ionization front velocity.

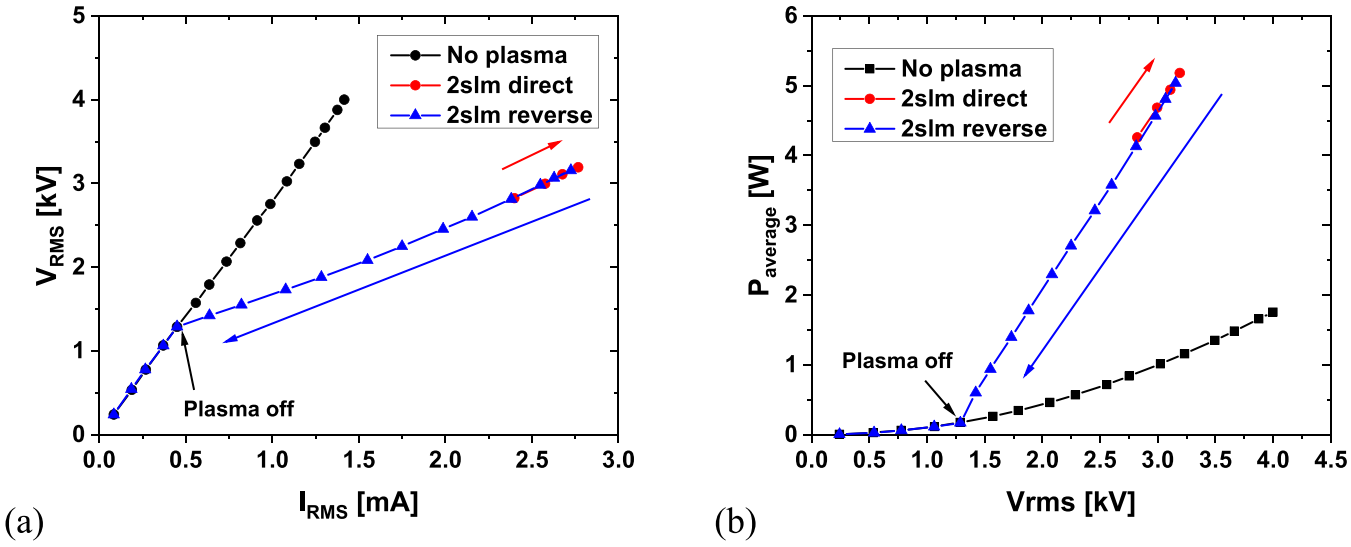


**Figure 3.** (a) Current voltage characteristics (b) power of the plasma jet as a function of $V_{RMS}$.

generators 1 and 2 with 80 kHz repetition rate. At the delay generator 2 (see figure 1) sine signal of 80 kHz was reduced to 20 Hz for the laser flash lamps and to 5 Hz for the laser Q-switch. The light from the interaction volume was collected by the lens (Avantes COL-UV/VIS) attached on the optical fiber (solarisation resistant) with a CCD spectrometer (AvaSpec-3648, spectral resolution 0.6 nm). The spectrometer was in a triggering mode with integration time of 10 $\mu$s. The laser focusing lens and optical fiber were mounted on the $y$ translator. The precision of the translators in $y$ axis direction was 10 $\mu$m and in $x$ axis direction 100 $\mu$m. The laser spot size was 80 $\mu$m. For more details, see [32].

The second experimental setup (figure 1(b)) for the ICCD measurements was previously described in paper [35], with some minor differences. The oscilloscope used here was Agilent DSO 6052a and high voltage probe was Tektronix P6015A, with 75 MHz bandwidth. For the current measurement we used 100× voltage probe (Agilent 10076B) for measurement of the voltage drop at the 100 kΩ resistor. For ICCD time resolved imaging we used Andor iStar DH734I ICCD camera and the plasma jet was in the horizontal position. Optical emission spectrum of the capillary plasma jet was measured using USB spectrometer Ocean Optics Maya2000 Pro (spectral resolution 0.5 nm).

## 3. Results and discussion

### *3.1. Electrical properties of the capillary plasma jet*

Plasma jet properties are highly dependent on the electrode configuration [36]. With that in mind, we first performed a detailed electrical analysis. The current and voltage signals for

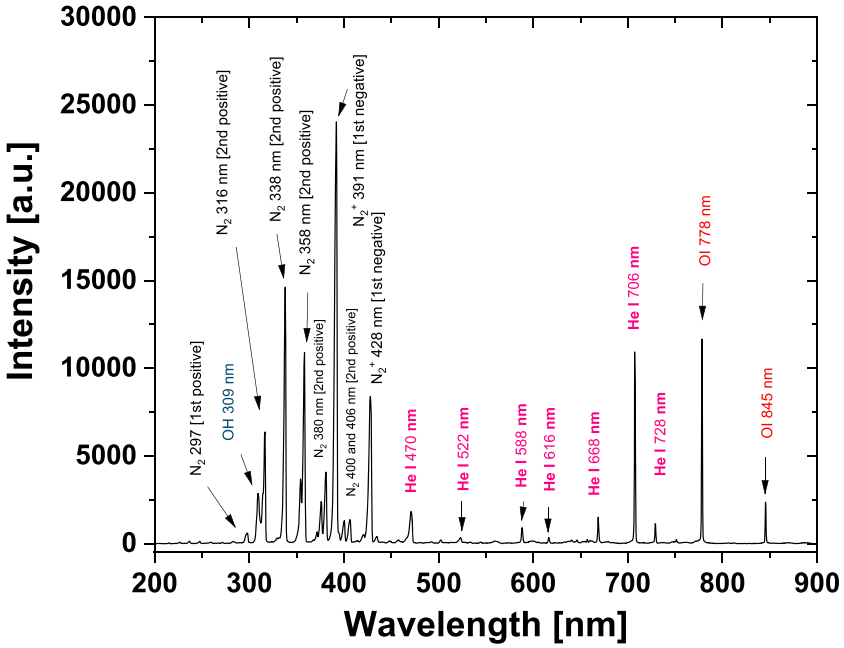


**Figure 4.** Typical OES spectrum for the helium plasma jet, for 2 slm helium, measured 5 mm below the plasma jet nozzle with 4 W of RF power delivered to the plasma.

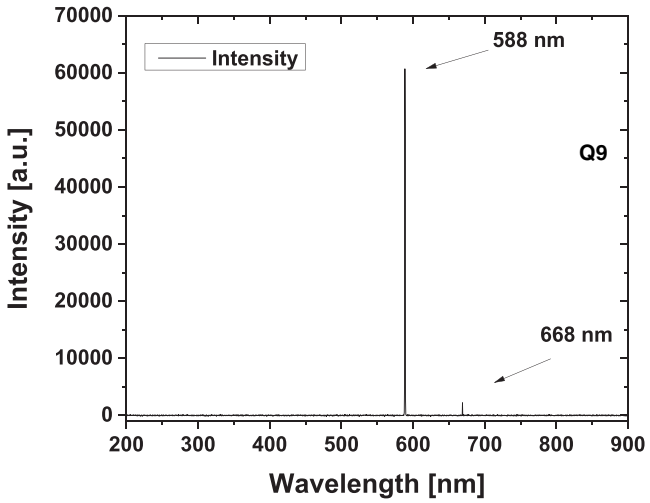


**Figure 5.** LIP spectrum in helium flow: 588 nm ($2p\ ^3P^\circ$–$3d\ ^3D$) and 668 nm ($2p\ ^1P^\circ$–$3d\ ^1D$) lines are observed. Helium flow was 2 slm, plasma was induced by the laser 5 mm from the jet nozzle, and 4 W of RF power was delivered to the plasma, the same as in figure 4. Since spectrum in figure 4 was recorded with a different spectrometer (Maya2000Pro) units of the intensity in figures 4 and 5 are completely different.

the plasma jet are shown in figure 2. In figure 2(a) current and voltage waveforms are presented, with the current and voltage waveforms captured at the main high voltage powering cable at the closest point to the powered electrode of the plasma jet. Peak to peak (p–p) values for current ($I$) were 20 mA and for the voltage ($V$) were 8.0 kV. The phase difference was close to $\pi/2$ (84°).

In figure 2(b) current and voltage waveforms for the plasma jet are presented. The voltage waveform was recorded near the powered electrode and the current waveform was recorded as the voltage drop on the resistor near the grounded electrode as presented in Maletić *et al* [35]. The measured p–p value of the current was 6.92 mA and of the voltage was 8.0 kV. If we compare the current waveforms at these two different points of the plasma jet (on the HV power cable and at the resistor), we can see almost three-time (3×) difference in its magnitude. The phase difference between voltage and the current was significantly lower than the current signal measured at the HV cable, it was 55°. The delay positions for the pulsed atmospheric pressure streamers (PAPS [16]) velocity calculation are shown in the figure 2 with circle symbol for the current and square symbol for the voltage. For this capillary plasma jet we can see two peaks superimposed on the current waveform. These peaks can be attributed to the collection of wall charges ($Q$) on the inner surface of the glass tube in the zone of powered and grounded electrode. In our previous experiments we could not observe the peak in the negative half cycle [35].

The $V$–$I$ characteristics are given in figure 3(a) as well as the power (in figure 3(b)) as a function of $V_{\mathrm{RMS}}$. The voltage was measured at the HV cable while the current was calculated from measured voltage drop at the 100 kΩ resistor. The calculated impedance for the plasma jet when the 'plasma is off' (without the working gas) was $Z = 2.80$ MΩ, while after plasma formation in the gas flow the impedance decreased to $Z = 0.81$ MΩ. We measured $V$–$I$ characteristics from the plasma ignition to the maximum power that our power supply can deliver and in the reverse direction until the plasma was extinguished. The power for the plasma jet is presented in figure 3(b). The power range for the capillary jet was narrow in direct direction (increasing power) just 1 W (from 4.2 to 5.2 W), while in reverse direction (decreasing power) the range was around 4.7 W (from 5.2 to 0.5 W).

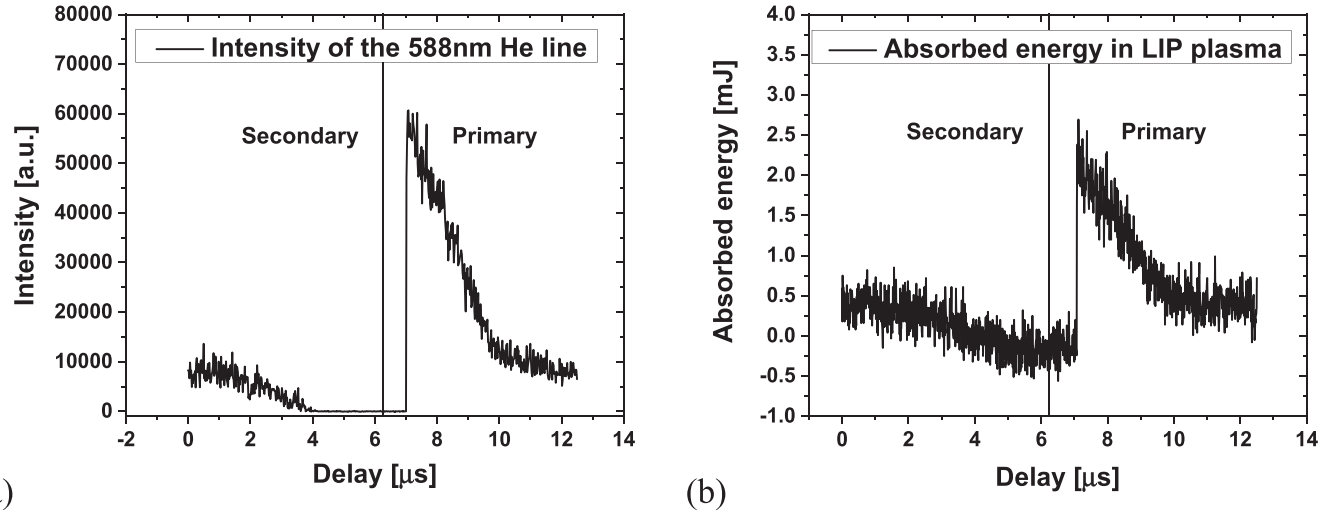


**Figure 6.** (a) Intensity of helium 588 nm line emission as a function of delay (intensity of emission was integrated over 10 $\mu$s and the entire volume of the induced plasma; (b) absorbed laser energy by the plasma jet as a function of the delay of laser trigger. Helium flow was 2 slm, Laser was focused at 5 mm from the jet nozzle, and 4 W of RF power was delivered to the plasma.

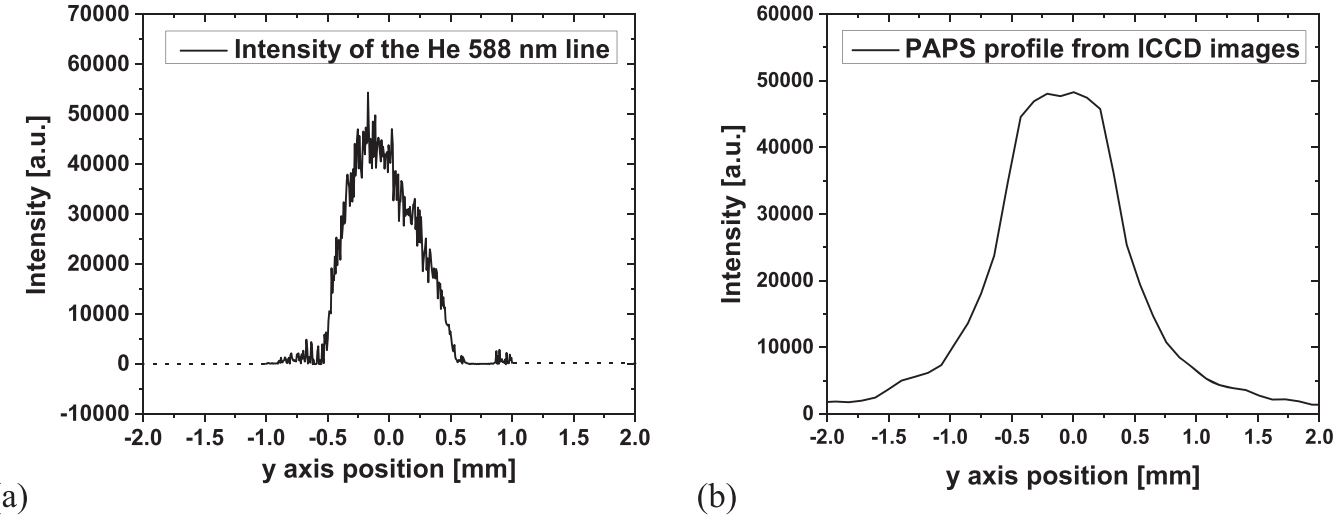


**Figure 7.** (a) Intensity of the He 588 nm line in the *y* axis, (b) total emission profile from the ICCD image. Helium flow 2 slm, 5 mm from the jet nozzle, 4 W of RF power delivered to the plasma. [ *y* axis is perpendicular to the axis of the gas flow and it is along the axis defined by the laser beam (radial position in reference Popović *et al* 2019 [32]). Measurements are performed by moving the focal point of the laser along the *y* axis.].

### *3.2. Time resolved emission intensity and absorbed laser energy by the plasma jet*

In air the laser induced breakdown occurred at about 10 mJ at room temperature (22 °C and with 25% relative humidity). The laser breakdown in air was accompanied with strong visible light from the spark and loud sound from the associated shock wave. When we focused the laser beam in the flow of helium coming from the plasma jet nozzle the breakdown occurred at a much higher laser pulse energy around 30 mJ with much less light emission and weaker sound [32]. When the laser energy was set to 20 mJ, the laser plasma was not induced since there were no seed electrons from the plasma jet present. Light emission from the plasma jet was around 1000 times weaker than the light from the LIP. Typical optical emission spectrum with 400 ms integration time for the helium plasma jet is shown in figure 4. The spectrum was recorded for the 4 W of RF power delivered to the plasma, 2 slm of helium and at the 5 mm in front of the plasma jet nozzle. He I, $N_2$, $N_2^+$, OH and OI lines may be observed in the spectrum of the free plasma jet. The He 588 nm line has a very weak intensity that was drastically increased in the LIP.

In figure 5 typical LIP spectrum is presented for the primary discharge (delay 7.08 $\mu$s), where one can observe two helium lines, 588 nm ($2p\ ^3P^\circ$–$3d\ ^3D$) and 668 nm ($2p\ ^1P^\circ$–$3d\ ^1D$). Integration time for the spectrometer was 10 $\mu$s. For the further plasma jet diagnostics, we chose the 588 nm line because of its strongest intensity. Molecular lines originating from the plasma jet could hardly be noticed since the LIP was

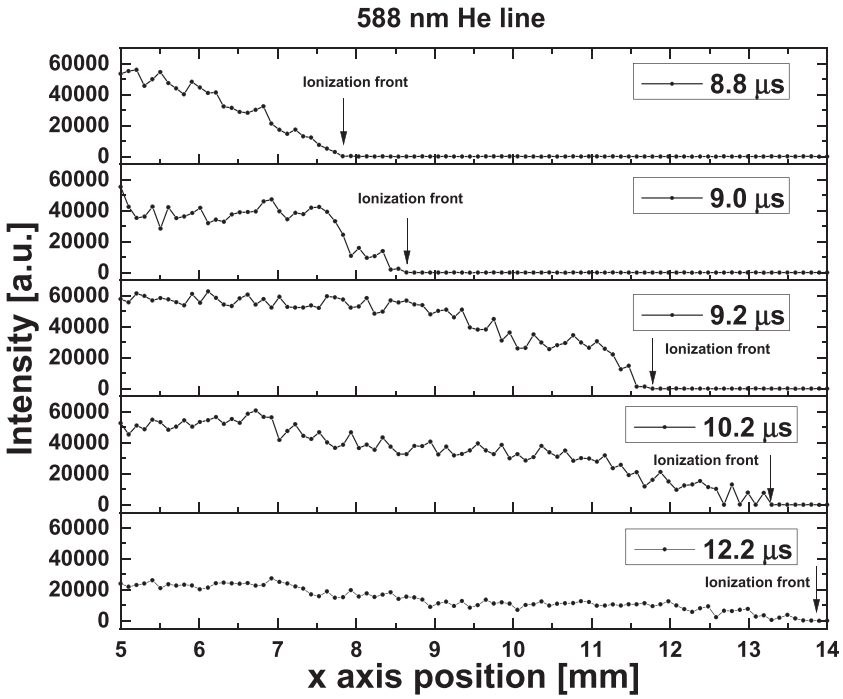


**Figure 8.** Emission profiles along the $x$ axis (distance from the capillary orifice) for different delays, the LIP is formed outside the glass tube. Helium flow was 2 slm, 4 W of power was delivered to the plasma.

producing emission that was several order of magnitude more intense in helium atmosphere.

In figure 6(a) we presented the intensities of the 588 nm He line for different delays of the laser–plasma jet synchronization. The position of the LIP was at 5 mm from the jet nozzle. As one can see the line intensities are dependent on the plasma jet voltages. The 0 $\mu$s correspond to 0 mA current, the voltage was around 3.0 kV in the falling slope (see figure 2(b)). This emission corresponds to the current peak in the negative half-cycle (secondary PAPS). When current starts to rise we can observe a sharp emission increase that corresponds to the current peak in the positive half-cycle (primary PAPS). The primary and secondary PAPS are typical for pulsed DC plasma jets [32]. The secondary PAPS was not observed with ICCD measurements (see figure 9) due to insufficient concentrations of seed electrons for the helium excitation in negative half-cycle of the excitation signal. In contrast to this LIP amplifies the emission signal of helium line, so the secondary PAPS were visible in emission spectrum of plasma jet. The difference in intensities between the positive and negative half cycles is around a factor of six (6×). Absorbed laser energy as the function of delay is shown in figure 6(b). We have the same shape of the absorbed light as for the light emission. One could argue that one can observe a smaller peak for the negative and a larger peak for the positive half-cycle. However, it is hard to make such a conclusion due to a different nature of the measurement of absorption and emission. The maximum absorbed laser energy in LIP plasma was 2.5 mJ.

### *3.3. Comparison of the plasma jet profiles obtained by LIP and ICCD measurement*

In figure 7 we show emission profile of the plasma jet at 5 mm from the jet nozzle. As one can see, the profile obtained with the LIP was considerably narrower than the profile from the ICCD images. The broad ICCD profile (figure 7(b)) is due to the light emission from plasma (helium in the center and nitrogen on the outer region of the jet) while the narrower (figure 7(a)) profile is due to the LIP intensity dependence on electron densities in helium flow. One should note that the LIP emission profile is not deconvoluted. Laser focal depth in direction of $y$-axis was estimated to be about 200 $\mu$m. From these two profiles one can estimate the size of the transitional region between the pure helium plasma and the surrounding air. The transitional region has a considerably weaker intensity of He lines than the emission in pure helium plasma. The size of the region with a high concentration of helium was $\pm$0.5 mm (in figure 7(a)) from the jet axis, and the transition region where most chemical reactions are occurring was around 1 mm on both sides beyond the He region. We did not observe any light emission further than $\pm$1.75 mm (in figure 7(b)) from the jet axis.

### *3.4. Comparison of the velocities for the plasma jet obtained with LIP and ICCD measurements*

In this paragraph we calculate the PAPS velocities using the edge of the emission in the axis of plasma jet propagation. The intensities of the 588 nm He line for different delays are shown in figure 8. The procedure for the PAPS velocity cal-

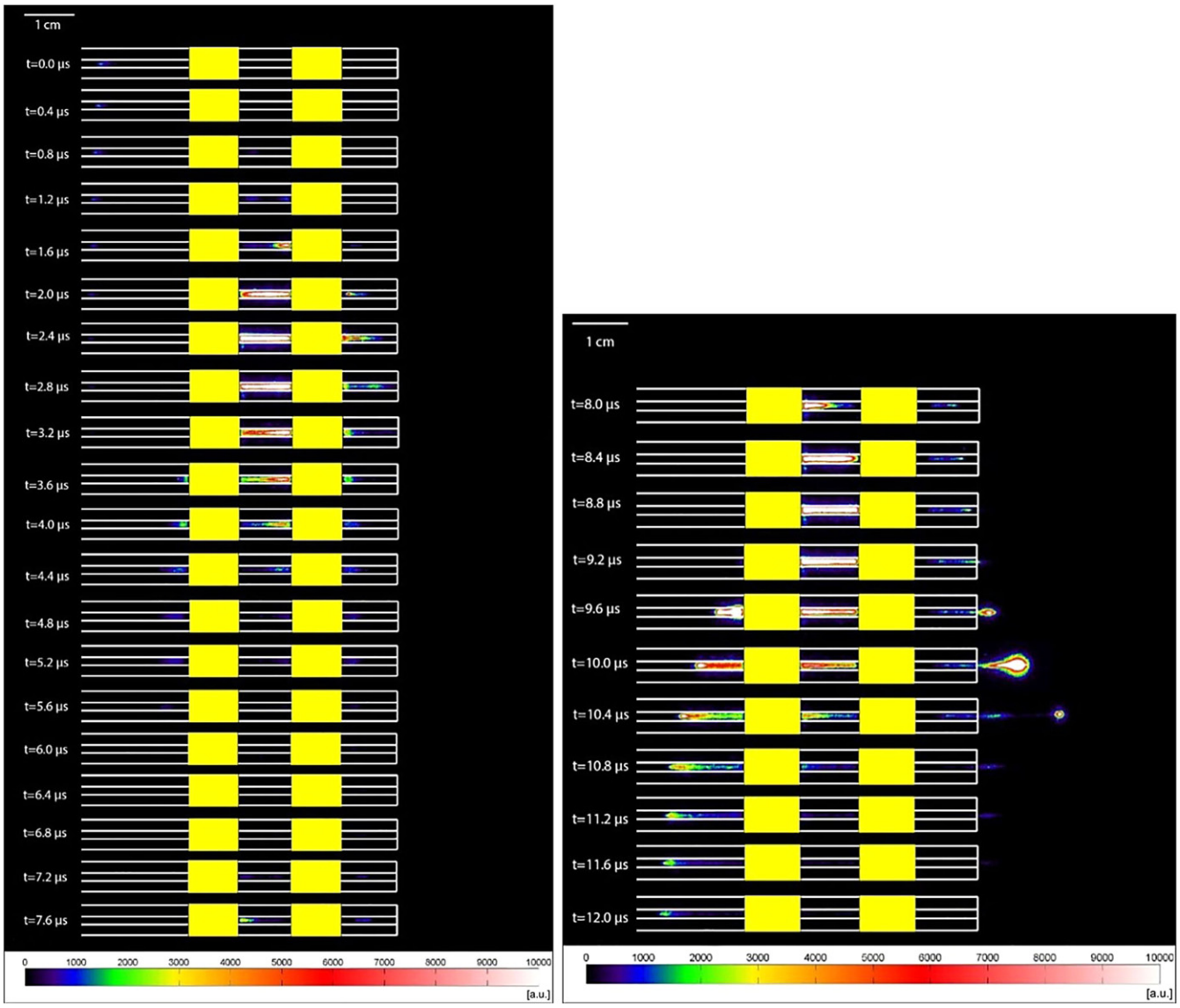


**Figure 9.** Time resolved broadband ICCD images of the capillary plasma jet for the whole period of the excitation signal, helium flow was 2 slm, 4 W of RF power were delivered to the plasma, gate width was 25 ns, exposure time 2 ms and gain was 200. Recording was made by integration on the chip of the ICCD.

culation is the following: (1) laser beam was focused in the center of the plasma jet; (2) the starting position of the LIP was 5 mm from the jet nozzle (0 on the $x$ axis); (3) plasma jet was translated along the $x$ axis; (4) for the fixed delay we recorded profiles; (5) for the velocity calculation we used position when the emission intensity drops to zero and that is the edge of the ionization front (marked with arrows in figure 8). As delay was varied we scanned different parts of the propagating front and thus we observed propagation of the emission front along the $x$ axis.

In figure 9 we have shown the ICCD images of the capillary plasma jet for the whole period of the excitation time. Left electrode was grounded and the right electrode was powered. We used integration on chip because of the very low light signal from the single period. The exposure time was 2 ms (160 periods), the gate width was 25 ns and the gain was 200. The starting delay position was when the current was zero. As one can see, the formation of the plasma in the negative half cycle occurred at 1.6 $\mu$s at the right edge of the powered electrode. Moving further in time the plasma filled the inter-electrode gap with high emission intensity. We have observed low intensity plasma in front of the powered electrode. Positive half-cycle starts at 8.0 $\mu$s (voltage waveform) and plasma was first formed at the left edge of the grounded electrode. The PAPS was formed at 9.6 $\mu$s, and propagated into the ambient air. At the same time another PAPS was formed at the right edge of the grounded electrode. This 'negative' PAPS was propagating in the opposite direction from the working gas flow. This kind of propagation was not observed in our previous experiments when we used glass tubes with larger I.D. (4 mm) [35].

In figure 10 we show velocities of the ionization fronts of the plasma jet outside the glass tube. The PAPS velocities (squares in figure 10) were calculated from the helium 588 nm

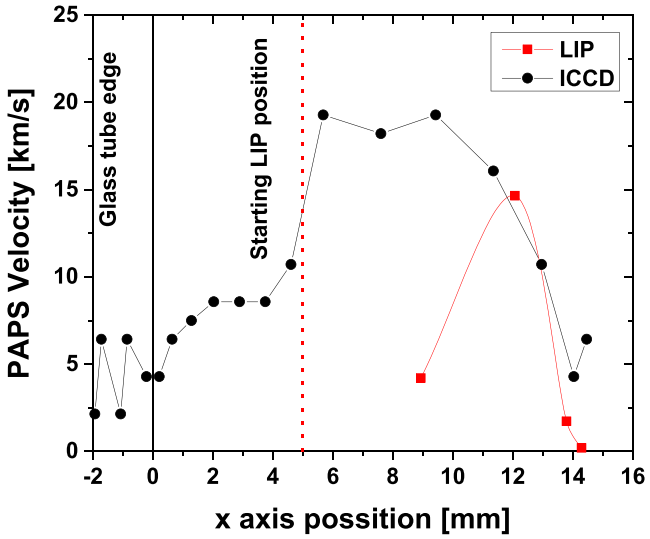


**Figure 10.** LIP PAPS velocities calculated from He line intensity and PAPS velocities calculated from ICCD images (100 ns step), helium flow was 2 slm, breakdown was induced at 5 mm from the jet nozzle and 4 W of RF power were delivered to the plasma.

line intensity propagation in space (see figure 8), the positions from the jet nozzle were calculated as $x$ position plus 5 mm (starting LIP position). We calculated that the maximal speed of the ionization front to be around 15 km $s^{-1}$. On the other hand, we show velocities of the IW (circles in figure 10) obtained from the fast ICCD images with the step of 0.1 $\mu$s (ICCD images are not presented). The maximal velocity obtained with this method is more precise and it is around the 20 km $s^{-1}$. One can see that the ionization front starts slowly to accelerate after the moment when PAPS leaves the glass tube up to 4 mm. After that point there is a rapid mixing of helium with the surrounding air and that leads to fast acceleration to the maximal front velocity 10 mm away from the nozzle. After reaching maximal velocity, ionization front velocity slowly decreases until plasma is extinguished at 15 mm from the nozzle. The estimated experimental errors for LIP and ICCD velocities calculation are under 10%.

Having in mind the accuracy of the LIP technique the two sets of results are in agreement. LIP diagnostics provides additional freedom to determine radial profile and observe a finer view of the inner structure of the propagating jet, especially the radial profile of mixing with air.

## 4. Conclusion

In this research paper we presented electrical properties, LIP and time resolved ICCD images for the capillary helium plasma jet driven by kHz sine waveform.

For this plasma jet we observed a large hysteresis effect when we decreased the power. We also observed the appearance of a peak (2 $\mu$s) in the current signal in the negative (falling) half-cycle and with LIP formation detect the presence of charge carrier near the jet nozzle. In the positive (rising) half cycle plasma jet front propagated inside the narrow glass tube against the flow.

We show that the LIBS (running at laser energy below threshold in helium) can be used for time resolved and spatial diagnostic of the APPJ. This method can be used as a complementary method for the diagnostics of plasma jets together with ICCD measurements, or independently. Using the LIP, we detected the secondary PAPS in negative half cycle of the excitation signal, we determined the dimensions of plasma channel with sufficient charge carriers necessary for initiation of the laser induced breakdown. Thus one may provide a profile of helium plasma mixing with air. Reasonable agreement of the two sets of results gives us confidence to claim that one may be able to use LIP to establish anatomy of more complex plasma systems. The LIP technique can be used together with LIF (or intra cavity spectroscopy) required to detect atoms and radicals produced in the plasma.

## Acknowledgments

This research has been supported by the Ministry of Education, Science and Technological Development, Republic of Serbia, under Grant No. 451-03-68/2020-14/200024 and Center of Excellence Non Equilibrium Processes, IPB. DM is also grateful for the funding of STSM in COST action TD1208 and to the Croatian Science Foundation HrZZ—IP-2019-04-6418. One of the authors (ZLP) is grateful to SASA project F155 and to Ulster University, U.K. SM and DP are grateful to the Croatian Science Foundation, through project IP-2013-11-2753.

## Data availability statement

The data that support the findings of this study are available upon reasonable request from the authors. Q10

## ORCID iDs

Dejan Maletić https://orcid.org/0000-0002-0368-6568
Dean Popović https://orcid.org/0000-0003-3906-3482
Zoran Lj Petrović https://orcid.org/0000-0001-6569-9447
Slobodan Milošević https://orcid.org/0000-0002-4455-7869

## References

[1] Petrović Z L, Puač N, Lazović S, Maletić D, Spasić K and Malović G 2012 *J. Phys.: Conf. Ser.* **356** 012001 Q11
[2] Bradley J W, Oh J-S, Olabanji O T, Hale C, Mariani R and Kontis K 2011 *IEEE Trans. Plasma Sci.* **39** 2312–3
[3] Maletić D, Puač N, Lazović S, Malović G, Gans T, Schulz-von der Gathen V and Petrović Z L 2012 *Plasma Phys. Control. Fusion* **54** 124046
[4] Oh J-S, Walsh J L and Bradley J W 2012 *Plasma Sources Sci. Technol.* **21** 034020
[5] Oh J-S, Furuta H, Hatta A and Bradley J W 2015 *Japan. J. Appl. Phys.* **54** 01AA03
[6] Zaplotnik R, Bišćan M, Krstulović N, Popović D and Milošević S 2015 *Plasma Sources Sci. Technol.* **24** 054004

[7] Boeuf J-P, Yang L L and Pitchford L C 2013 *J. Phys. D: Appl. Phys.* **46** 015201
[8] Li J, Lei B, Wang J, Zhang T, Tang J, Wang Y, Zhao W and Duan Y 2019 *IEEE Trans. Plasma Sci.* **47** 3134–40
[9] Emmert S *et al* 2013 *Clin. Plasma Med.* **1** 24–9
[10] Wu S, Wang Z, Huang Q, Tan X, Lu X and Ostrikov K 2013 *Phys. Plasmas* **20** 023503
[11] Ghimire B *et al* 2019 *Appl. Phys. Lett.* **114** 093701
Q12 [12] Oh , Szili , Hatta , Ito and Shirafuji 2019 *Plasma* **2** 127–37
[13] Cheng X, Sherman J, Murphy W, Ratovitski E, Canady J and Keidar M 2014 *PLoS One* **9** 1–9
[14] Fröhling A, Baier M, Ehlbeck J, Knorr D and Schlter O 2012 *Innov. Food Sci. Emerg. Technol.* **13** 142–50
[15] Nastuta A V, Topala I, Grigoras C, Pohoata V and Popa G 2011 *J. Phys. D: Appl. Phys.* **44** 105204
[16] Ghasemi M, Olszewski P, Bradley J W and Walsh J L 2013 *J. Phys. D: Appl. Phys.* **46** 052001
[17] Kim J Y and Kim S-O 2011 *IEEE Trans. Plasma Sci.* **39** 2278–9
[18] Wang R, Xu H, Zhao Y, Zhu W, Zhang C and Shao T 2019 *Plasma Chem. Plasma Process.* **39** 187–203
[19] Lamichhane P, Paneru R, Nguyen L N, Lim J S, Bhartiya P, Adhikari B C, Mumtaz S and Choi E H 2020 *React. Chem. Eng.* **5** 2053–7
[20] Royintarat T, Seesuriyachan P, Boonyawan D, Choi E H and Wattanutchariya W 2019 *Curr. Appl. Phys.* **19** 1006–14
[21] Gierczik K, Vukušić T, Kovcs L, Szkely A, Szalai G, Milošević S, Kocsy G, Kutasi K and Galiba G 2020 *Plasma Process. Polym* **17** 1900123
[22] Kutasi K, Popović D, Krstulović N and Milošević S 2019 *Plasma Sources Sci. Technol.* **28** 095010
[23] Tanaka H, Mizuno M, Ishikawa K, Nakamura K, Kajiyama H, Kano H, Kikkawa F and Hori M 2011 *Plasma Med.* **1** 265–77
[24] Tomić S, Petrović A, Puač N, Škoro N, Bekić M, Petrović Z L and Čolić M 2021 *Cancers* **13** 1626
[25] Adamovich I *et al* 2017 *J. Phys. D: Appl. Phys.* **50** 323001
[26] Puač N, Gherardi M and Shiratani M 2018 *Plasma Process. Polym.* **15** 1700174
[27] Hahn D W and Omenetto N 2012 *Appl. Spectrosc.* **66** 347–419
[28] Burger M, Skočić M and Bukvić S 2014 *Spectrochim. Acta* B **101** 51–6
[29] Barreda F-A, Trichard F, Barbier S, Gilon N and Saint-Jalmes L 2012 *Anal. Bioanal. Chem.* **403** 2601–10
[30] Ji H, Ding Y, Zhang L, Hu Y and Zhong X 2021 *Appl. Spectrosc. Rev.* **56** 193–220
[31] Morgan C G 1975 *Rep. Prog. Phys.* **38** 621–65
[32] Popović D, Bišćan M and Milošević S 2019 *Plasma Sources Sci. Technol.* **28** 055009
[33] Woodbury D, Schwartz R M and Milchberg H M 2019 *Optica* **6** 811
[34] Gott R P and Xu K G 2020 *J. Phys. D: Appl. Phys.* **53** 315201
[35] Maletić D, Puač N, Selaković N, Lazović S, Malović G, Dorđević A and Petrović Z L 2015 *Plasma Sources Sci. Technol.* **24** 025006
[36] Maletić D, Puač N, Malović G, Dorđević A and Petrović Z L 2017 *J. Phys. D: Appl. Phys.* **50** 145202
[37] Karakas E, Akman M A and Laroussi M 2012 *Plasma Sources Sci. Technol.* **21** 034016